Convective Assembly of 2D Lattices of Virus-like Particles Visualized by In-Situ Grazing-Incidence Small-Angle X-Ray Scattering

Carlee E. Ashley, Darren R. Dunphy, Zhang Jiang, Eric C. Carnes, Zhen Yuan, Dimiter N. Petsev, Plamen B. Atanassov, Orlin D. Velev, Michael Sprung, Jin Wang, David S. Peabody, and C. Jeffrey Brinker*

The rapid assembly of icosohedral virus-like particles (VLPs) into highly ordered (domain size > 600 nm), oriented 2D superlattices directly onto a solid substrate using convective coating is demonstrated. In-situ grazing-incidence small-angle X-ray scattering (GISAXS) is used to follow the self-assembly process in real time to characterize the mechanism of superlattice formation, with the ultimate goal of tailoring film deposition conditions to optimize long-range order. From water, GISAXS data are consistent with a transport-limited assembly process where convective flow directs assembly of VLPs into a lattice oriented with respect to the water drying line. Addition of a nonvolatile solvent (glycerol) modified this assembly pathway, resulting in non-oriented superlattices with improved long-range order. Modification of electrostatic conditions (solution ionic strength, substrate charge) also alters assembly behavior; however, a comparison of in-situ assembly data between VLPs derived from the bacteriophages MS2 and Qβ show that this assembly process is not fully described by a simple Derjaguin–Landau–Verwey–Overbeek model alone.

1. Introduction

The use of viral particles (including icosahedral and filamentous bacterial phages, as well as plant viruses[1] as building blocks or scaffolds in the synthesis of nanoscale materials presents several distinct advantages over the use of 'synthetic' nanoparticles. These include the nearly perfect monodispersity of size and shape, convenience of synthesis from laboratory culture, and most importantly, the ability to

Dr. C. E. Ashley,[+,++] Prof. D. R. Dunphy,[+] Prof. E. C. Carnes,
Dr. Z. Yuan,[+++] Prof. D. N. Petsev, Prof. P. B. Atanassov
University of New Mexico/NSF Center for Micro-Engineered Materials
Department of Chemical and Nuclear Engineering
Albuquerque, NM, 87131, USA

Dr. Z. Jiang, Dr. M. Sprung,[++++] Dr. J. Wang
Advanced Photon Source
Argonne National Laboratory
Argonne, IL, 60439, USA

Prof. O. D. Velev
North Carolina State University
Department of Chemical and Biomolecular Engineering
Raleigh, NC, 27695, USA

Prof. D. S. Peabody
University of New Mexico
Molecular Genetics and Microbiology
Albuquerque, NM, 87131, USA

Prof. C. J. Brinker
Sandia National Laboratories
Advanced Materials Laboratory
Albuquerque, NM, 87106, USA
Email: cjbrink@sandia.gov

[+] These authors have contributed equally to this work.
[++] Current address: Sandia National Laboratories, Livermore, CA, 94550, USA
[+++] Current address: Symyx Technologies, Santa Clara, CA, 95051, USA
[++++] Current address: HASYLAB at DESY, Hamburg, 22607, Germany

selectively modify the viral structure with organic or inorganic substances through encapsidation of nanoparticles[2] or other foreign materials within the internal volume of the particle and conjugation of functional peptides (either through chemical reaction or genetic engineering) to selectively bind or nucleate the growth of inorganic materials at the surface of the viral capsid.[1,3] By combining these particle modification approaches with self-assembly into periodic 2- and 3D arrays, viral particles could, in principle, be used as scaffolds, templates, or 'nanocontainers' to organize virtually any type of functional inorganic material into larger hierarchical structures relevant to energy transduction, sensing, information storage, logic devices, etc.[1–3] Practical fabrication of such functional assemblies requires a continuous and rapid coating method applicable to large-scale solid substrates; although 3D crystallization,[4] liquid crystal alignment,[5] and interfacial assembly[6] have been investigated as means of viral organization, direct assembly of highly ordered 2D viral superlattices at the solid/air interface remains an essential goal. Here, using *convective assembly*[4,7,8] (CA), we demonstrate the continuous formation of 2D hexagonal superlattices of virus-like particles (VLPs), derived from the icosohedral bacteriophages MS2 and Qβ, directly onto silicon substrates, with domain sizes extending beyond 600 nm. Although CA has been used to deposit films of the rodlike tobacco mosaic virus (TMV),[8] no true superlattice was formed, with the only degree of film-ordering arising from (imperfect) shear alignment of the TMV particles along the direction of coating. Importantly, as optimization of superlattice order as well as future design of nonhexagonal particle packing requires a fundamental understanding of the self-assembly mechanism, we used grazing-incidence small-angle X-ray scattering (GISAXS) at a synchrotron source to monitor the assembly process in situ, finding that the precise VLP assembly pathway (convective, diffusive, surface adsorption) is highly dependent on experimental conditions. Beyond serving as a means of fabricating VLP superlattice templates for further material organization, these results are an important insight into nanoparticle self-assembly processes occurring at length scales where the synthesis of monodisperse particles is experimentally difficult.

CA has emerged as a promising tool for the rapid, generalized deposition of colloidal assemblies directly onto a solid surface. In CA (**Figure 1**), a film is deposited from a microliter-sized droplet of a colloidal suspension trapped between a fixed substrate and a plate translated at constant velocity v across the substrate at a fixed angle θ (typically < 30°). For spherical colloidal particles, assembly is driven by convective transport to the drying line induced by evaporation combined with interparticle capillary forces.[9] In general, the role of electrostatic and van der Waals forces in the assembly process is significant only in that interparticle and particle–surface interactions can suppress the formation of an ordered lattice.[10] Here, we extend this method to icosohedral VLPs (capsids assembled from viral coat protein without the presence of genetic material) derived from the ca. 28 nm bacteriophages MS2 and Qβ (**Figure 2**). Icosahedral viruses and VLPs present a number of unique properties as nanoscale building blocks arrays when compared to TMV or other filamentous phages,
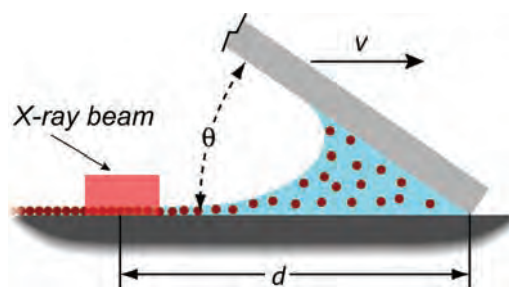

Figure 1. Schematic of the convective assembly process used in GISAXS studies of VLP self-assembly. A plate at angle θ is moved across a substrate at velocity v, entraining a meniscus from which a particle film is deposited. The self-assembly process is probed at a fixed position on the substrate denoted by the shaded area; d is the time-dependent distance between the X-ray beam and the edge of the coater.

including almost spherical symmetry and nearly perfect monodispersity (enabling the assembly of highly ordered crystalline superlattices[6]), and the ability to produce VLPs from plasmids in *E. coli* in large quantities.[11] Also, the availability of improved genetic screens and selections[12] relative to those available for rodlike viruses could eventually allow the identification of mutants with tailored interaction potentials or the ability to direct specific growth of inorganic materials.

In contrast to electron microscopy (a technique generally limited to ex-situ studies[13,14]) or optical methods, GISAXS enables the in-situ characterization of nanostructure during dynamic assembly processes in real-time under ambient environments and over large areas.[14–16] In GISAXS, an X-ray beam is incident upon a sample at an angle greater than the critical angle of the film but less than that of the substrate, thus maximizing the scattering volume inside the film.
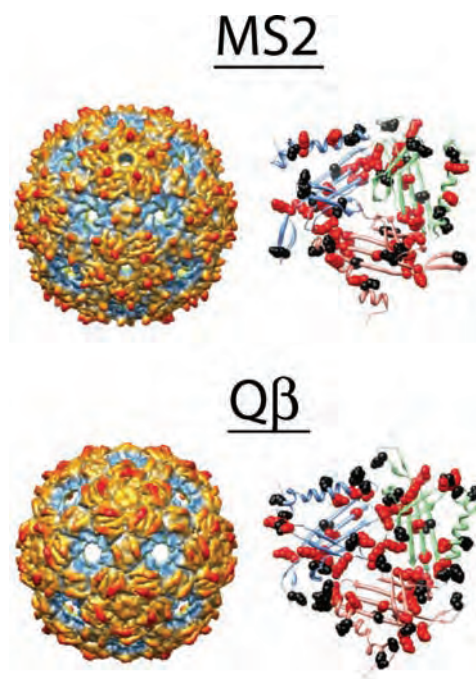

Figure 2. Structures of Qβ and MS2 bacteriophages (left), and close-ups of phage subunit structure for Qβ and MS2 (right), with acidic and basic amino acid residues highlighted in red and black, respectively.

Coupled with the high photon flux obtained at a synchrotron source, it enables the investigation of fast (on the time scale of seconds) self-assembly phenomena of films as thin as one monolayer.[14,16] For the study of CA, the X-ray beam is maintained at a fixed position upon the solid substrate (Figure 1); the film assembly process is monitored as the plate of the convective coater passes through and past this position.

2. Results and Discussion

2.1. Convective Assembly from H$_2$O

Our initial studies compared the CA of VLPs derived from MS2 and Qβ (Figure 2). MS2 and Qβ are nearly identical in size (with a diameter of 27.5 nm for MS2 and 28.5 nm for Qβ), but differ in the overall number of ionizable surface residues,[17] charge distribution (both radially from the center of the particle and across the surface, with Qβ exhibiting a more uniform coverage across each capsid subunit as compared to MS2, where charge is concentrated at subunit edges),[17] and acidity (with isoelectric points of pH = 3.9 and 5.3 for MS2 and Qβ, respectively). As seen in the time-sequence in-situ GISAXS data in **Figure 3**, these differences result in dissimilar self-assembly behavior; however, it is not clear at this time what specific structural features are responsible for this disparity in behavior. In this data, time is referenced to the first appearance of a particle array (panels b and f). For both particle types, the initial scattering is dominated by a grazing-incidence reflection from the curved liquid meniscus and glass slide of the convective coater (panels a and b). A set of cross-hatched scattering features also appears (most notably in the data set for MS2) that we do not attribute to any self-assembly process given the symmetry of these features with the background reflection. For Qβ, the self-assembly process can be divided into two stages; direct appearance (panel b) and evolution (panel c) of a close-packed superlattice monolayer, notably without any intermediate structure, followed by a reduction in film ordering from water evaporation and imposition of capillary stresses (panel d). Prior to the complete drying of water (panels a and b), the 2D lattices of the particles are at the liquid/substrate interface, confirming the convection-induced self-assembly mechanism. Parenthetically, we note that, if the self-assembly were to occur at the air/liquid interface, the scattering patterns would be drastically different, with the rodlike features of the GISAXS data in panels b and f appearing perpendicular to the curved air/liquid interface.[14,16] Upon complete drying of the water (panel d), the in-plane order is significantly reduced as indicated by the broadening of the scattering peaks. MS2 assembly is characterized by an initial formation of a 2D superlattice (panel f), with subsequent structural development during film drying dominated by a transition to multilayer aggregates (panel g), leaving a glassy film (panel h) with reduced long-range order when compared to Qβ. This propensity toward aggregation for MS2 is a result of the electrostatic properties of this particle, a conclusion supported by assembly as a function of ionic strength (vide infra).
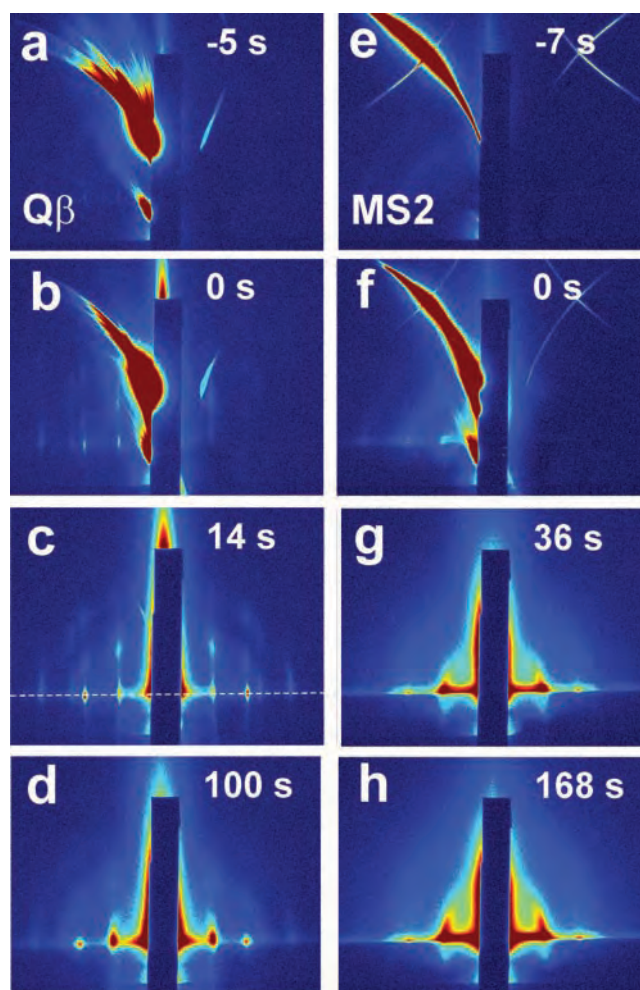

Figure 3. Time sequence of GISAXS data, referenced to the first emergence of the X-ray beam from behind the plate of the convective coater (a,e), comparing the self-assembly of Qβ (a–d) and MS2 (e–h) from deionized (DI) water under identical coating conditions. For Qβ, assembly of 2D arrays occurs without intermediate aggregation or structure formation (b,c); weakened and broader (20) and (21) reflections indicate loss of long-range order during the final stage of film drying (d). MS2 assembly is characterized by poor long-range order in comparison to Qβ (g), including the formation of a glassy multilayer film upon H$_2$O evaporation (h) and a much smaller domain size. Plate movement is from left to right in both series of images.

The well-ordered (defined by GISAXS data with narrow peak widths and multiple scattering orders) superlattice of Qβ allows for more detailed analysis of assembly dynamics; data for Qβ assembly was analyzed as presented in **Figure 4**a–c. Line cuts plotted versus time (panel b) show a broadening of the (10) diffraction peak as well as a shift to higher q (with q being the magnitude of the scattering vector, in units of nm^{-1}) during film drying. The (10) peak shape analysis in the beginning at time, $t = 19$ s shows a lattice constant of 24.2 nm (giving an interparticle spacing of $24.2 * (2/\sqrt{3}) = 28.0$ nm, consistent with the size of Qβ, indicating a closely packed monolayer with a domain size of ~280 nm, estimated using the Scherrer equation from the full width at half maximum (FWHM) of the (10) peak. Similar analysis near the end at $t = 162$ s shows a contracted packing, with lattice constant of 22.3 nm
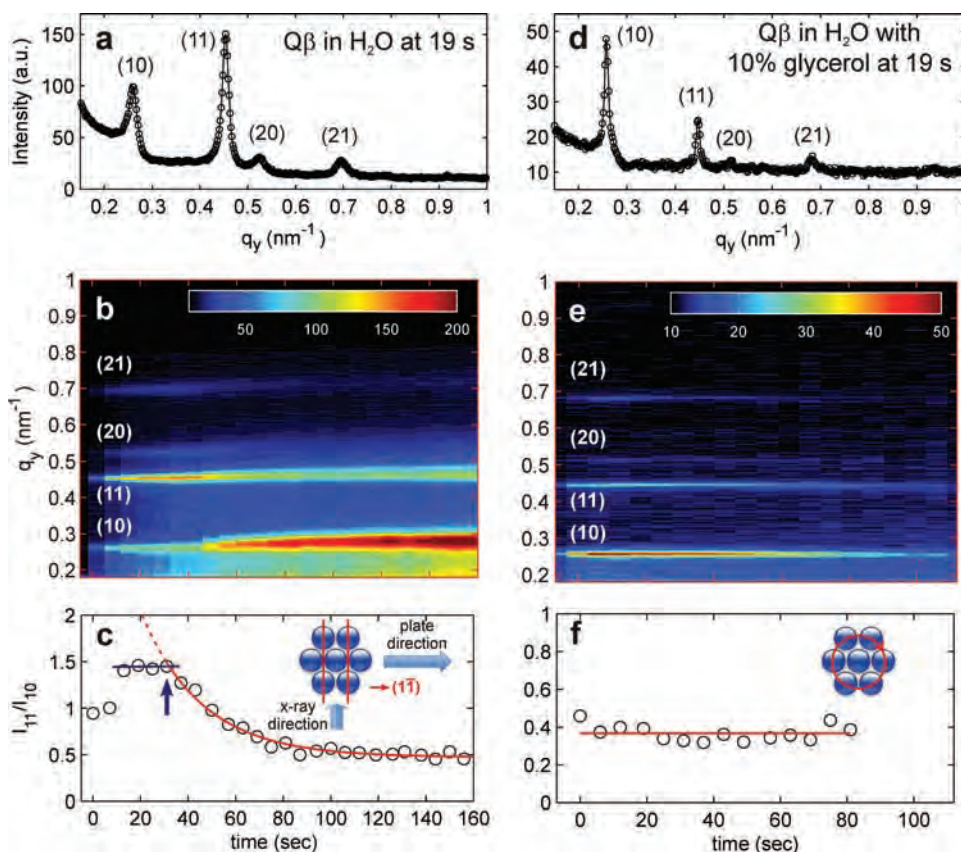
Figure 4. a) A horizontal linecut at $q_z = 0.24 \pm 0.02$ nm^{-1} taken from the GISAXS data for Qβ self-assembled in DI water at $t = 19$ s (the dashed line marked in Figure 3c). The first four Bragg diffractions are indexed to 2D hexagonal packing. b) The time evolution of this horizontal linecut. c) The ratio of the integrated intensities underneath the (11) and (10) reflections, after background subtraction. The red line is a fit to an exponential decay function as described in the text, and the inset represents the dominant 2D domain orientation induced by convective transport. d–f) The corresponding panels from GISAXS for Qβ in water with 10% glycerol.

(an interparticle distance of 25.7 nm) and an average domain size of ~158 nm. We attribute this shrinkage in interparticle spacing during film drying to compression and deformation of the (empty) VLP capsid. The average number of particles per domain also decreases by 60% during film drying, from ca. 120 at $t = 19$ s to ca. 50 at $t = 162$ s, an effect of cracks and other defects which directly reduce domain size.

Figure 4c plots the intensity ratio of (11) and (10) reflections (I_{11}/I_{10}) from the data in panel b, revealing the assembly kinetics of the VLP superlattice. From this data, it is apparent that convective transport favors an orientation of the self-assembled domains with (11) direction parallel to the direction of the plate motion. This initial superlattice orientation is consistent with an assembly mechanism as seen with macroscopic particles whereby convective transport of particles toward a drying front, induced by water evaporation, is combined with immersion capillary forces to guide the packing of colloidal particles into a 2D lattice.[18] The observed reorientation of superlattice domains after assembly demonstrates that the film maintains fluidity over a time scale sufficient for structural rearrangement in the film, either by rotation of entire superlattice domains or diffusion of individual particles; the presence of either process suggests incomplete surface coverage of the 2D viral array. This

thermal diffusion can be fit to an exponential decay of the generalized form of $I_{11}/I_{10} = C_1 + C_2 e^{-t/\tau}$, giving a characteristic time scale τ of 26 ± 3 s, consistent with the onset time of 31 s (labeled with a blue arrow in panel 4c) for this diffusion mechanism to dominate the average orientation of the VLP domains. The peak intensity ratio saturates at a value of $C_1 = 0.47$, slightly smaller than 0.58 estimated from the simulations for randomly oriented 2D domains modeled using paracrystal theory,[19] an effect we attribute to the form factor of the VLP particles.

2.2. Convective Assembly from H$_2$O/Glycerol Mixtures

In contrast to Qβ assembly from H$_2$O, Qβ self-assembled in 10% glycerol (which, compared to water, has a 1000-fold higher viscosity and $>1 \times 10^6$ lower vapor pressure at 20 °C) has a nearly constant lattice parameter of 24.4 nm (interparticle distance is 28.2 nm), and a much higher degree of ordering, which is seen as much sharper diffractions in Figure 4d,e. The observed FWHM for these diffraction features are limited by our instrument resolution of ~0.01 nm^{-1}, indicating an averaged domain size beyond ~600 nm. Also, the ratio of (10) to (11) intensity is constant over time

(Figure 4e,f), with a value that suggests formation of random domain orientation within the film. We postulate that the lack of a favored domain orientation, along with the increased long-range order relative to films deposited from water without glycerol, is a result of a fundamentally different mechanism for superlattice assembly; specifically, we hypothesize a self-assembly mechanism where convective flow at the drying line is negligible due to an increase in viscosity in the coating solution after preferential evaporation of water as well as the inherent low volatility of glycerol. Instead, transport of particles to the growing superlattice is controlled by 2D diffusion. Although diffusion-controlled aggregation might be expected to produce open, fractal-like structures, simulations of 2D nanoparticle assembly have demonstrated that at high surface coverage and sufficiently long diffusion times, extended domains are formed,[20] consistent with our hypothesized assembly mechanism for VLPs in the presence of glycerol. We note that increased mobility at the substrate surface due to the presence of a nonvolatile medium cannot account for the increased order alone, as the rearrangement of superlattice orientation seen in Qβ films deposited from H$_2$O indicate significant surface mobility of particles without glycerol over the time frame of film formation. Another factor that may influence the degree of long-range order in assemblies of viral particles between glycerol and aqueous solutions is the Debye length of the virus. However, variation of the Debye length for Qβ during self-assembly by variation of the NaCl concentration (from 0.1 mM to 1.0 M, Debye length = 30 and 0.3 nm, respectively) did not show any increase in the degree of long-range ordering, suggesting that for Qβ electrostatic screening is not a significant factor in superlattice formation, again consistent with convective transport dominating the self-assembly process from aqueous solutions.[18] Reduction in immersion capillary forces during the 2D crystallization process between particles in water versus particles in glycerol may play a role in increased superlattice ordering; however the reduction in interparticle force in the latter case is expected to be only ca. 13%.[18]

2.3. Reduction of VLP Aggregation During Convective Assembly

Finally, we utilized our in-situ GISAXS studies of VLP assembly to examine the aggregation of MS2 during CA in more detail, with the ultimate goal of identifying assembly conditions that maximize 2D superlattice order for VLPs with greater interparticle interactions. Colloidal aggregation can be lessened by increasing the electrostatic repulsion between particles through the reduction of the ionic strength of the supporting medium, or by increasing the surface potential of the particles.[21] Consistent with these predictions, a study of assembly from NaCl solutions with ionic strengths between 10^{-6} and 1.0 M found that aggregation of MS2 was eliminated for NaCl concentrations below 100 mM, forming ordered 2D superlattices (**Figure 5**a–c). Assuming a tenfold concentration of electrolyte at the point of MS2 aggregation, this corresponds to a Debye length of ca. 1 nm, on the same length scale as the peptide loops extending from the surface of MS2.[17] Interestingly, along with the expected 2D hexagonal
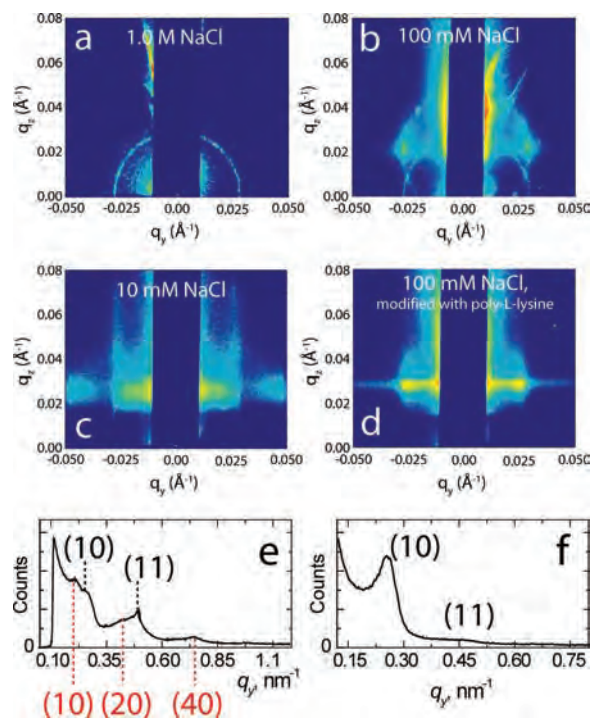

Figure 5. a–c) GISAXS data for MS2 assembled from 1.0, 100, and 10 mM NaCl solutions. d) GISAXS data for oligo-L-lysine-modified MS2 assembled from 100 mM NaCl, showing the formation of an ordered superlattice. e) Linecut ($q_z = 0.29 \pm 0.01$ nm^{-1}) for the data in (c), indicating the presence of two superlattice types. f) Linecut ($q_z = 0.29 \pm 0.01$ nm^{-1}) for the data in (d), clarifying the existence of 2D hexagonal packing.

structure, we find evidence of a second superlattice geometry (as seen in the linecut of the data in Figure 5c, which is given in Figure 5e) with a (10) spacing (31.4 nm) consistent with the presence of a non-close-packed superlattice; we note that bilayers of square packing have previously been observed in the assembly of colloidal particles by convective flow.[18] Also, we find that increasing the surface potential of MS2 by the addition of excess charge through chemical conjugation with decamers of the cationic peptides oligo-L-lysine or oligo-L-arginine inhibited aggregation of MS2, permitting the assembly of 2D close-packed superlattices from 100 mM NaCl onto oxidized silicon (Figure 5d, linecut in Figure 5f).

Although this observed reduction of MS2 aggregation with decreased ionic strength is qualitatively consistent with DLVO (Derjaguin–Landau–Verwey–Overbeek) theory,[22] the relative aggregation behavior between MS2 and Qβ is not readily explained, given that both of these VLPs are characterized by zeta potentials of less than –10 mV at pH 7, within the range where particle aggregation is expected for both VLP types.[23] At short interparticle distances, a simple description of particle–particle attraction may break down due to complex surface topography, as has been noted for protein–protein interactions,[24] as well as registration of charged residues and hydrophobic patches arising from the nonrandom distribution of these features across the VLP surface.

Assembly onto cationic or anionic amine- or carboxylate-modified self-assembled monolayers (SAMs) was also

found to reduce aggregation of MS2, while altering the self-assembly pathway for both MS2 and Qβ VLPs relative to that seen for superlattice formation at oxidized silicon. Example in-situ data for MS2 assembly at an amine-modified SAM in 100 mM NaCl is shown in **Figure 6**a–c; data for assembly at a carboxylic-acid-terminated interface as well as for Qβ at either surface is qualitatively similar. We find that superlattice development at an amine- or carboxylic-acid-terminated surface differs in several important respects over that seen at a hydroxyl-terminated silica surface. First, ordering in MS2 arrays is increased relative to that seen at unmodified surfaces under identical solution conditions as evidenced by the appearance of a (21) reflection (Figure 6b). Unlike assembly of Qβ at unmodified surfaces, the I_{11}/I_{10} ratio for both MS2 and Qβ is constant throughout the entire film formation process (equal to ca. 0.4, consistent with isotropic ordering of superlattice domains in the plane of the substrate) until complete film drying induces collapse of the VLP superlattice (Figure 6c). However, there are significant changes in interparticle spacing with the superlattice over time; as seen in Figure 6d and e for MS2 and Qβ, respectively, the (10) interplanar spacing undergoes expansion from an initial compacted state (Figure 6a, with an initial interparticle distance of ca. 26.5 nm for both MS2 and Qβ) to a lower packing density (Figure 6b, interparticle spacing is 27.3 nm on both surfaces for MS2, and 30.5 or 29.3 nm for Qβ on amine- and carboxylate-modified SAMs, respectively) followed by shrinkage of the superlattice during film drying (as was seen for Qβ assembly on silica) and, in the case of MS2, complete collapse of the film into a glassy state (Figure 6c).

Based upon this data, we postulate a mechanism for VLP assembly at an amine- or carboxylate-modified surface whereby VLP superlattice formation is preceded by adsorption of VLP to the SAM surface, with subsequent solvent evaporation inducing assembly into 2D hexagonal packing from interparticle and capillary interactions, as has been observed previously for nanoparticle assembly at a self-assembled monolayer.[25] Lack of observed solution precipitation (evidenced by the lack of an isotropic scattering ring in the X-ray data) of the MS2 suggests that this adsorption step occurs before solvent evaporation increases the VLP concentration to a point where MS2 interparticle aggregation occurs. During the adsorption step, the VLP capsid is compressed; expansion of the interparticle distance during film drying demonstrates fluidity and possible flattening of individual VLPs, along with incomplete surface coverage in the adsorbed VLP monolayer. The time-independent isotropic superlattice orientation indicates that convective transport is not a significant factor for MS2 assembly at these modified surfaces. For MS2, the presence of an ordered 2D structure is temporary, with complete film drying prompting superlattice collapse via aggregation.

3. Conclusion

In summary, we have demonstrated the formation of close-packed 2D superlattice monolayers of empty viral capsids though a convective coating technique, following the
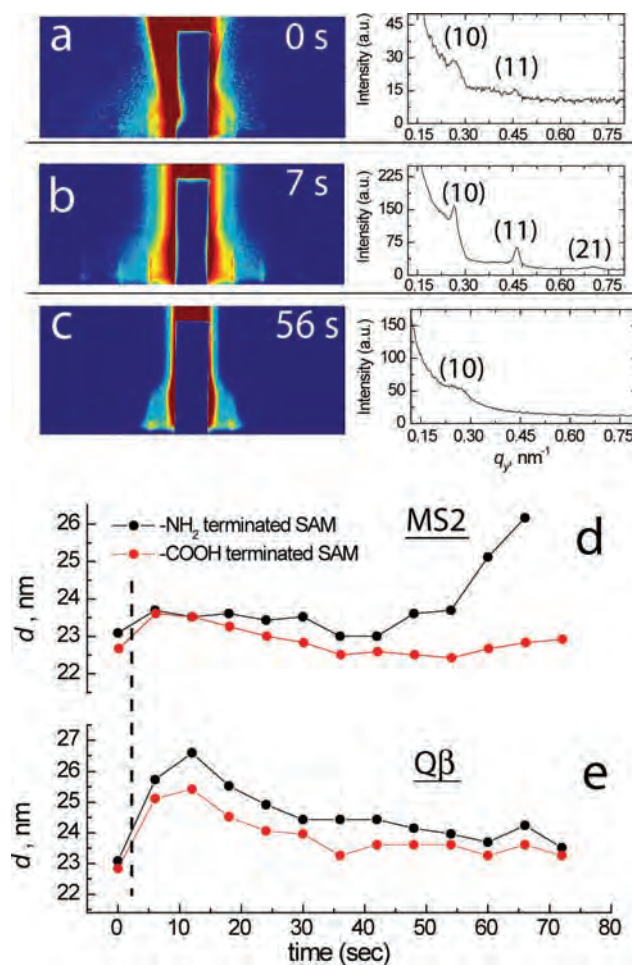

Figure 6. a–c) Time-sequence in-situ GISAXS data for the convective assembly of MS2 from 100 mM NaCl onto an amine-modified self-assembled monolayer, with initial appearance of the MS2 lattice (a), followed by development of lattice order (b), and ultimate collapse after film drying (c). d,e) Lattice spacing for the (10) reflection as a function of time for MS2 (d) and for Qβ (e) assembled at an amine- or carboxylate-terminated SAM.

self-assembly process in real time using grazing-incidence small-angle X-ray scattering at a synchrotron source. From water onto oxidized silicon, the assembly mechanism is consistent with convective transport of particles to the drying front of the evaporating film; scrambling of the superlattice orientation after the initial assembly stage shows the presence of fluidity in the VLP monolayer. Addition of nonvolatile solvent to the VLP solution increases domain size, with an invariant average superlattice orientation suggesting that assembly does not occur through convective transport, but possibly by random particle diffusion within the deposited film. Although 2D superlattice formation of MS2 was suppressed by solution aggregation under conditions that otherwise led to well-defined ordering of Qβ, we found that modification of ionic strength or MS2 surface potential enables the assembly of ordered assemblies. Finally, assembly onto a charged self-assembled monolayer appears to modify the self-assembly mechanism such that convective transport is replaced by surface adsorption, with interparticle aggregation

of VLP suppressed by competition with particle–surface interactions. Although we have achieved the assembly of highly ordered 2D lattices of viral particles, the most highly ordered superlattice states are only transitory; use of these VLP arrays to template inorganic materials formation will require methods to stabilize these phases, perhaps by modification of the VLP surface with cross-linking functionality.

4. Experimental Section

VLP Preparation: MS2 and Qβ bacteriophages were produced by infection of *Escherichia coli* A/λ using standard methods[26] and purified by sedimentation to equilibrium in CsCl gradients. Virus-like particles were produced from the parental bacteriophage via incubation in pH 11.8 buffer for 4 h, which hydrolyzes the RNA genome and results in empty capsids. VLPs were stored in TNME buffer (10 mM Tris-HCl, 100 mM NaCl, 0.1 mM MgSO$_4$, and 0.01 mM EDTA (ethylenediaminetetraacetic acid) at pH 7.4) at 4 °C. The following conditions were employed in all GISAXS measurements: particle volume fraction (ϕ) = 0.02, deposition velocity (v) = 12 μm s^{-1}, relative humidity during the coating process = 15%. Oligo-L-lysine and oligo-L-arginine (New England Peptide, each 10 peptides in length) were synthesized with a C-terminal cysteine moiety and chemically conjugated to lysine residues present on the exterior MS2 VLP surface using a thiol-cleavable heterobifunctional (amine-to-sulfhydryl) crosslinker (Sulfo-LC-SPDP, Pierce). VLPs were activated via incubation with a twofold molar excess of Sulfo-LC-SPDP for 1 h at room temperature, and unreacted crosslinker was removed using a centrifugal filtration device (100 kDa molecular-weight cut off). Activated VLP was then incubated with a tenfold molar excess of oligopeptide overnight at 4 °C; excess peptide was removed via centrifugal filtration. Average oligopeptide density was determined using Tricine SDS-PAGE; 10 mM dithiothreitol (DTT) was added to the sample buffer to liberate peptides from denatured phage proteins prior to electrophoresis. ImageJ Image Processing and Analysis Software was utilized to compare band intensities of electrophoresed peptides relative to a standard concentration curve: each MS2 VLP was estimated to bear 120 copies of oligo(Lys) or oligo(Arg).

In-Situ X-Ray Studies: GISAXS measurements were performed on beamline 8-ID at the Advanced Photon Source at Argonne National Labs using a wavelength of 1.6868 Å, a sample-to-detector distance of either 1580 or 1254 mm, an analysis angle of 0.20°, and a 2048 × 2048 Marr charge-coupled device (CCD) detector. The 100 μm × 50 μm beam was fixed relative to the substrate (Figure 1), with the beam direction perpendicular to the movement of the coater plate. Detector images were obtained with a period of 6 s, using an integration time of 1 s.

For production of Figure 2, images were rendered in Chimera using data obtained from VIPERdb.[17]

[1] M. Young, D. Willits, M. Uchida, T. Douglas, *Annu. Rev. Phytopathol.* **2008**, *46*, 361.

[2] S. E. Aniagyei, C. DuFort, C. C. Kao, B. Dragnea, *J. Mater. Chem.* **2008**, *18*, 3763.

[3] a) M. Fischlechner, E. Donath, *Angew. Chem. Int. Ed.* **2007**, *46*, 3184; b) A. Merzlyak, S. W. Lee, *Curr. Opin. Chem. Biol.* **2006**, *10*, 246.

[4] Y. G. Kuznetsov, A. J. Malkin, R. W. Lucas, M. Plomp, A. McPherson, *J. Gen. Virol.* **2001**, *82*, 2025.

[5] a) S. W. Lee, S. K. Lee, A. M. Belcher, *Adv. Mater.* **2003**, *15*, 689; b) S. W. Lee, C. B. Mao, C. E. Flynn, A. M. Belcher, *Science* **2002**, *296*, 892; c) S. W. Lee, B. M. Wood, A. M. Belcher, *Langmuir* **2003**, *19*, 1592.

[6] a) J. B. He, Z. W. Niu, R. Tangirala, J. Y. Wan, X. Y. Wei, G. Kaur, Q. Wang, G. Jutz, A. Boker, B. Lee, S. V. Pingali, P. Thiyagarajan, T. Emrick, T. P. Russell, *Langmuir* **2009**, *25*, 4979; b) G. Kaur, J. B. He, J. Xu, S. V. Pingali, G. Jutz, A. Boker, Z. W. Niu, T. Li, D. Rawlinson, T. Emrick, B. Lee, P. Thiyagarajan, T. P. Russell, Q. Wang, *Langmuir* **2009**, *25*, 5168; c) J. T. Russell, Y. Lin, A. Boker, L. Su, P. Carl, H. Zettl, J. B. He, K. Sill, R. Tangirala, T. Emrick, K. Littrell, P. Thiyagarajan, D. Cookson, A. Fery, Q. Wang, T. P. Russell, *Angew. Chem. Int. Ed.* **2005**, *44*, 2420.

[7] a) B. G. Prevo, J. C. Fuller, O. D. Velev, *Chem. Mater.* **2005**, *17*, 28; b) B. G. Prevo, Y. Hwang, O. D. Velev, *Chem. Mater.* **2005**, *17*, 3642; c) B. G. Prevo, O. D. Velev, *Langmuir* **2004**, *20*, 2099.

[8] S. P. Wargacki, B. Pate, R. A. Vaia, *Langmuir* **2008**, *24*, 5439.

[9] B. G. Prevo, D. M. Kuncicky, O. D. Velev, *Colloid. Surface A* **2007**, *311*, 2.

[10] Z. Yuan, D. N. Petsev, B. G. Prevo, O. D. Velev, P. Atanassov, *Langmuir* **2007**, *23*, 5498.

[11] D. S. Peabody, *J. Biol. Chem.* **1990**, *265*, 5684.

[12] D. S. Peabody, B. Manifold-Wheeler, A. Medford, S. K. Jordan, J. do Carmo Calderia, B. Chackerian, *J. Mol. Biol.* **2008**, *380*, 252.

[13] a) T. P. Bigoni, X.-M. Lin, T. T. Nguyen, E. I. Corwin, T. A. Witten, H. M. Jaeger, *Nat. Mater.* **2006**, *5*, 265; b) X.-M. Lin, H. M. Jaeger, C. M. Sorensen, K. J. Klabunde, *J. Phys. Chem. B* **2001**, *105*, 3353; c) D. G. Schulz, X.-M. Lin, D. Li, J. Gebhardt, M. Meron, P. J. Viccaro, B. Lin, *J. Phys. Chem. B* **2006**, *110*, 24522.

[14] S. Narayanan, J. Wang, X.-M. Lin, *Phys. Rev. Lett.* **2004**, *93*.

[15] a) D. Dunphy, H. Y. Fan, X. F. Li, J. Wang, C. J. Brinker, *Langmuir* **2008**, *24*, 10575; b) S. V. Roth, T. Autenrieth, G. Gruebel, C. Riekel, M. Burghammer, R. Hengstler, L. Schulz, P. Mueller-Buschbaum, *Appl. Phys. Lett.* **2007**, *91*, 091915.

[16] Z. Jiang, X.-M. Lin, M. Sprung, S. Narayanan, J. Wang, *Nano Lett.* **2010**, *10*, 799.

[17] M. Carrillo-Tripp, C. M. Shepherd, I. A. Borelli, S. Venkataraman, G. Lander, P. Natarajan, J. E. Johnson, C. Brooks, L., V. S. Reddy, *Nucleic Acids Res.* **2009**, *37*, D436.

[18] N. D. Denkov, O. D. Velev, P. A. Kralchevsky, I. B. Ivanov, H. Yoshimura, K. Nagayama, *Langmuir* **1992**, *8*, 3183.

[19] R. Hosemann, S. N. Bagchi, *Direct Analysis of Diffraction by Matter*, North-Holland Publishing, Amsterdam, **1962**.